# Large-Area Protein Patterns Generated by Ordered Binary Colloidal Assemblies as Templates

**Gurvinder Singh,[†] Vipul Gohri,[‡] Saju Pillai,[§] Ayyoob Arpanaei,[⊥] Morten Foss,[†] and Peter Kingshott[¶,*]**

[†]Interdisciplinary Nanoscience Center (iNANO), Aarhus University, Ny Munkegade, Building 1521, 8000 Aarhus C, Denmark, [‡]Microoled, 7 parvis Louis Neel Grenoble Cedex 38040, France, [§]Department of Mechanical Engineering, Aalborg University, Aalborg 9220, Denmark, [⊥]Department of Industrial and Environmental Biotechnology, National Institute of Genetic Engineering and Biotechnology, P.O. Box 14965/161, Tehran, Iran, and [¶]Industrial Research Institute Swinburne (IRIS), Faculty of Engineering and Industrial Sciences, Swinburne University of Technology, Hawthorn, 3122 VIC, Australia

**ABSTRACT** We demonstrate the use of binary colloidal assemblies as lithographic masks to generate tunable Au patterns on $SiO_2$ substrates with dimensions ranging from micrometers to nanometers. Such patterns can be modified with different chemistries to create patterns with well-defined sites for selective adsorption of proteins, where the pattern size and spacing is adjustable depending on particle choice. In our system, the binary colloidal assemblies contain large and small particles of similar or different material and are self-assembled from dilute dispersions with particle size ratios ranging from 0.10 to 0.50. This allows masks with variable morphology and thus production of chemical patterns of tunable geometry. Finally, the Au or $SiO_2$ regions of the pattern are surface modified with protein resistant oligoethyleneglycol self-assembled molecules, which facilitates site selective adsorption of proteins into the unmodified regions of the pattern. This we show with fluorescently labeled bovine serum albumin.

**KEYWORDS:** protein patterning · self-assembly · binary colloidal assembly · binary colloidal lithography · nanofabrication · surface functionalization

The generation of chemically patterned surfaces with multiple length scales on flat surfaces for selective immobilization of biomolecules is an active area of research in nanobiotechnology.[1] Such surfaces have numerous biological and medical applications in areas including biosensors and bioanalytics, tissue engineering, microarray technology, drug screening, and fundamental studies of cell biology.[2−9] For example, there is a substantial interest in gaining a fundamental understanding of the cell−artificial surface interactions mediated *via* the protein adlayer and how this relates to subsequent cellular responses, wound healing, and tissue integration.[10] Chemically patterned surfaces provide an ideal platform to study various cellular functions such as attachment, proliferation, differentiation, and apoptosis through variations of pattern geometry and chemistry.[11−14] However, the accurate and controlled immobilization of low concentrations or even individual biomolecules on a surface remains a key challenge, restricting both the study and application of protein based devices. Therefore, a primary goal is to develop simple, robust, and cheap approaches to biomolecule patterning from length scale ranges from micrometers to a few nanometers over relatively large areas.

Over the past few decades, several strategies for chemical patterning have been developed such as conventional photolithography,[15] soft lithography,[16]scanning near-field optical lithography,[17] dip-pen lithography,[18] imprint lithography,[19] and electron beam lithography,[20] to name a few. Some drawbacks of these methods include molecular intercalation, side reactions, and use of harsh solvents; thus, the quality, resolution, and further activity of biological species on the patterned surface are affected adversely.[21] Although these methods have generated very valuable knowledge of how to pattern different materials and in subsequent biological studies, they also suffer some limitations. These include low throughput, limits to the choice of deposited materials, high costs, they can be time-consuming, and some of them require complex instrumentation, which limits availability to many laboratories. Colloidal lithography (CL) has emerged as an alternative technique that has the potential to overcome several of these limitations.[22] This lithographic technique uses a self-assembled colloidal crystal monolayer as a mask for depositing various metals,[23] catalysts,[24] polymers,[25] and inorganic materials on surfaces.[26] The advantages associated with CL are that it does not require direct access to conventional lithographic equipment, and can be easily integrated with existing material deposition techniques such as sputtering/evaporation,[27]

* Address correspondence to pkingshott@groupwise.swin.edu.au.

Received for review October 24, 2010 and accepted April 15, 2011.

**Published online April 15, 2011**
**10.1021/nn102867z**

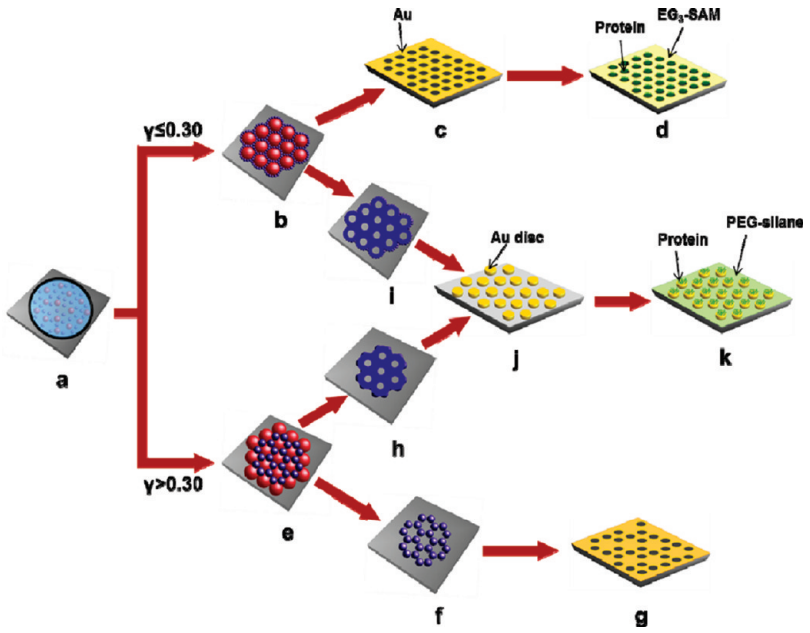


**Figure 1. Schematic illustration showing the generation of different chemical patterns from low and high size ratio BCAs, and subsequent protein patterning after surface modification of the patterned surface. (a) A mixed suspension of different sizes of colloidal particles is spread inside a rubber ring. (b,e) BCAs form after complete evaporation of the solvent. (c) Au sputtering over the colloidal mask and the removal of particles by sonication or lift-off yield chemically patterned surfaces. (f) Heating the composite template made from PS and $SiO_2$ particles for 5 to 10 min at 100 °C and removal of $SiO_2$ particles by HF treatment. (g) Au deposition over the mask generates a chemical pattern comprising six holes arranged in hexagonal fashion. (h, i) Heating the composite masks for longer duration (20−45 min) at 120 °C and removal of silica particles by HF etching. (j) Au deposition and subsequent removal of PS particles yield disklike gold patterns. (d, k) The chemical modification of the patterned surface with protein resistant molecules guides the specific adsorption of the protein to unmodified regions.**

chemical vapor deposition,[28] reactive ion etching,[29] and plasma polymerization to produce chemical patterns of desired chemistry.[30,31] Recently, CL has also shown its capability to generate non-close-packed patterns on planar and nonplanar supports,[32−35] and direct patterning of biomolecules or quantum dots without any need for deposition techniques.[36−38] A possible limitation of CL is the use of colloidal particles of sizes below 200 nm that can lead to short-range ordering with several defects or particle aggregates, which severely affects the quality of subsequent chemical patterns.[39]

To challenge this limitation we employ binary colloidal assemblies (BCAs) as a lithographic mask. The self-assembly of large particles is facilitated by the small particles and produces well-ordered colloidal masks with fewer numbers of defects and works well with nanoparticles.[31] The self-assembly of binary colloidal particles produces tunable masks depending on the size ratios ($\gamma$ = small to large) of particles used, which facilitates versatile chemical patterns with controllable spacings down to the nanoscale. In addition, composite BCAs made from, for example, polystyrene (PS), and silica ($SiO_2$) particles, can also be used as a mask after PS or $SiO_2$ particles are selectively etched away. Although, several methods have been studied for the controlled growth of different binary colloidal crystals, including evaporation-induced self-assembly,[40] stepwise spin coating,[41] and template-assisted assembly,[42] we find that the long-range ordering of binary crystals can be achieved by employing a modified method proposed by Denkov *et al.* (1992).[43] Here, the colloidal solution was confined inside a ring to grow monolayers of monocomponent colloidal crystals. Recently, we showed that a binary colloidal mask could be successfully used to form nanoscale patterns by combining BCAs ($\gamma \leq 0.30$) with plasma polymerization.[31] Our objective in this study was to change the chemical pattern geometry by using different and composite BCAs (both low and high size ratios) as lithographic masks, and utilize them to adsorb proteins selectively after surface modification. Different chemical micro- and nanopatterns can be created by exposing the templates to sputter-coating processes. Sputtering is a less directional deposition process compared to evaporation and does not cause any shadowing effect, thus enabling the formation of continuous patterns.[44] For this study, Au was chosen as the depositing material (foreground pattern) on the silicon/glass substrates (background) due to its unique chemical and optical properties and uses in biological applications.[45−47] In addition, various protein immobilization strategies have also been developed for gold surfaces to preserve protein conformation and activity.[48] The patterned surfaces were further subjected to selective adsorption of biomolecules after chemical modification with protein resistant molecules, for example, 1-(mercapto-11-undecyl)-tri(ethylene glycol) ($EG_3$-SAM)

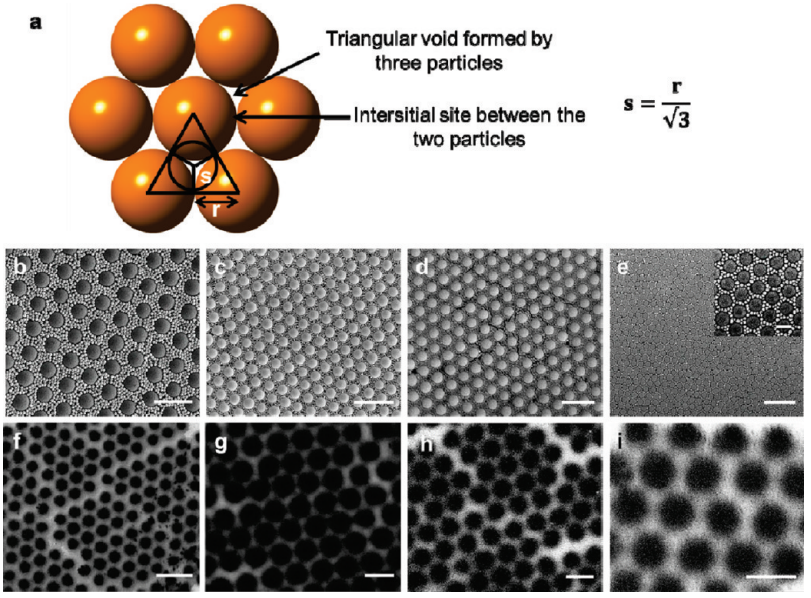


**Figure 2. (a) Schematic representation of the interstitial sites made by the monolayer of large particles where *s* and *r* refer to the radius of inscribed circle and the large particle, respectively. SEM micrographs show BCAs at low size ratio (*i.e.*, $\gamma \leq 0.30$). (b) 2 $\mu$m COOH−PS ($\varphi = 5.3 \times 10^{-4}$) and 200 nm $NH_2$−PS ($\varphi = 9.5 \times 10^{-5}$); scale bar = 3 $\mu$m. (c) 1 $\mu$m $SO_4$−PS ($\varphi = 2.7 \times 10^{-4}$) and 110 nm $NH_2$−PS ($\varphi = 5.6 \times 10^{-5}$); scale bar = 3 $\mu$m. (d) 500 nm $NH_2$−PS ($\varphi = 1.1 \times 10^{-4}$) and 60 nm COOH−PS ($\varphi = 9.5 \times 10^{-5}$); scale bar = 1 $\mu$m. (e) 200 nm $NH_2$−PS ($\varphi = 6.6 \times 10^{-5}$) and 60 nm COOH−PS ($\varphi = 9.4 \times 10^{-5}$); scale bar = 1 $\mu$m (inset scale bar = 200 nm). "$\varphi$" refers to volume fraction of the particle. Au against $SiO_2$ patterns in panels f−i correspond to the BCA shown immediately above them in panels b−e: (f) *t* = 10 min, scale bar = 4 $\mu$m, (g) *t* = 10 min, scale bar = 1 $\mu$m, (h) *t* = 5 min, scale bar = 500 nm, and (i) *t* = 5 min, scale bar = 200 nm.**

and 2-[methoxy-(polyethylene glycol)propyl]trichlorosilane (PEG-silane), which was verified using X-ray photoelectron spectroscopy (XPS).

## RESULTS AND DISCUSSION

Figure 1 shows a systematic illustration of tunable patterns from low and high size ratio BCAs. In step 1, a binary colloidal suspension in highly purified deionized water is drop-cast inside a rubber ring fixed onto a clean hydrophilic surface (Figure 1a). The mechanism of its formation is described elsewhere,[31] but briefly, the highly ordered BCAs are formed as a consequence of capillary and convective flow forces after complete evaporation of solvent.[43] In addition, electrostatic repulsive forces also acted between the particles either in suspension or on the substrate and prevent aggregation during the assembly formation until entropic induced crystallization occurs at the last stages of solvent evaporation.[49] We did not observe any size separation or clustering of particles after mixing two different sized colloidal particles. This may be explained by calculating a depletion interaction energy ($\sim 0.003 K_B T$, where $K_B$ is the Boltzmann constant and $T$ is the temperature), which is much lower than an electrostatic energy ($\sim 10^3 K_B T$) for the 2 $\mu$m COOH−PS and 200 nm $NH_2$−PS ($\gamma$ = 0.10) system at all interparticle separations (see Text in the Supporting Information). Notably, varieties of BCAs are observed after the complete evaporation of a colloidal suspension inside the ring (Figure 2b−e). The formation of these binary crystals depends highly on the size ratio and concentration of the particles employed during the self-assembly process; although we have not studied the role of the particle concentration ratio on BCA formation, previous studies have shown this effect.[40,50,51] However, our main finding is that the size ratio has also a larger influence on the type of BCA when a very low concentration of small particles is insufficient to completely cover the substrate. Thus, geometrical packing constraints or size ratio dictates the arrangement of small particles in the interstices within the monolayer of large particles.

The small particles can assemble in two different interstices of the particles including the triangular voids generated from the three large neighboring particles, and the channels between the two large neighboring particles (Figure 2a). At low size ratio ($\gamma$ = 0.10) and for 2 $\mu$m COOH−PS, the size of small particles (200 nm $NH_2$−PS) is much less than the theoretical diameter of the inscribed circle (~1155 nm). Therefore, several small particles freely move in the free space available within the large colloidal crystal layer, and evaporation of the solvent from voids causes them to settle over both the interstices (*i.e.*, triangular void and channel between the two large particles) of the large particles arranged in hexagonal fashion (Figure 2b). Here, we did not see a complete coverage of the large particles by the small particles because the capillary forces arising from menisci formation around the large particles are strong enough to overcome an electrostatic attractive

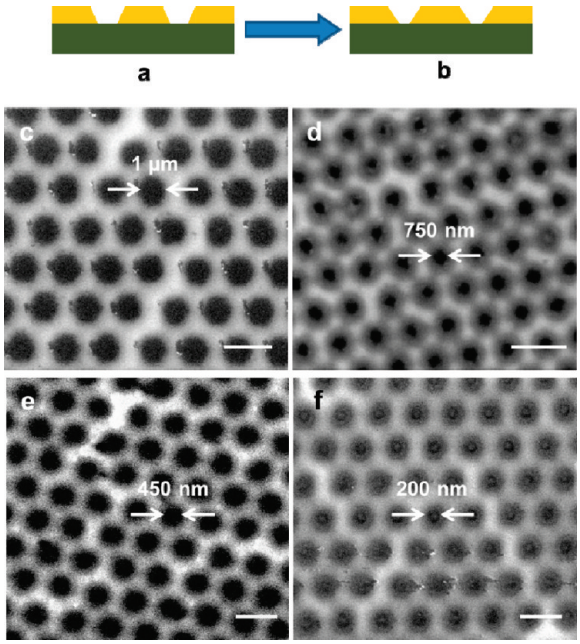


**Figure 3. (a, b) Schematic diagram shows the effect of deposition time (*t*) on the lateral dimensions of the patterned surfaces ($Au/SiO_2$). SEM micrographs show reduction in the lateral dimension and morphological changes in chemical patterns produced from 2 $\mu$m COOH−PS/200 nm $NH_2$−PS binary colloidal masks (c) *t* = 10 min, scale bar = 2 $\mu$m; (d) *t* = 20 min, scale bar = 3 $\mu$m; and 1 $\mu$m $SO_4$−PS/110 nm $NH_2$−PS (e) *t* = 10 min, scale bar = 1 $\mu$m; (f) *t* = 20 min, scale bar = 1 $\mu$m.**

interaction between the primary amines and carboxylic groups and drive the small particles into interstices.[43] Some previous reports have theoretically described a so-called "halo effect" which claims that the small particles stabilize the large particles in suspension preventing accumulation.[52] Similar results were also obtained for other low size ratio values (Figure 2c,d). As $\gamma$ increases to 0.20 or above, interstices of large particles are uniformly packed by a single layer of the smaller particles (Figure 2e). Here, the theoretical diameter of the inscribed circle (~115 nm) is two-times larger than the size of small particles. In all cases a monolayer of the large particles are formed and their contact to the substrate provides a template for pattern formation. The larger versions of SEM micrographs (Figure 2b−e) are also displayed in the Supporting Information (see Figures S1−S4). Once the assemblies are created, they are exposed to a Au sputtering source and the chemically patterned surfaces result after the removal of the binary colloidal mask by either lift-off (by tape stripping) or sonication in solvent (Figure 1c,g,j). The surface modification of chemical patterns with protein resistant molecules directs the specific adsorption of biomolecules to unmodified regions (Figure 1d,k).

The series of scanning electron microscopy (SEM) micrographs (Figure 2f−i) are evidence of Au against $SiO_2$ (silicon substrate) chemical patterns produced from the different BCA masks ($\gamma \leq 0.30$). A longer deposition time produces clear contrast between the Au and substrate. A Au patterned surface generated from 2 $\mu$m COOH−PS and 200 nm $NH_2$−PS shows lower height areas (holes) of ~1 $\mu$m diameter located in an array corresponding to the original array of the large particles (Figure 2f). It is noteworthy that the diameters of these holes are less than the diameters of the large particles because of the shadowing exerted by the large particles. It may be understood considering the bimodal kinetic energy distribution of gas-phase atoms proposed by Haynes *et al.*[45] According to this model, low kinetic energy atoms (~0.1 eV) travel along direct line-of-sight. In contrast, only high energy (~1 to 20 eV) atoms that travel along off-normal trajectories strike the substrate. Thus, this effect is thought to be due to diffusion that enables energetic species to undergo some "sideways" movement and the film form underneath "ledges" created by large particles. These high energy atoms may also be responsible for the off-normal axis Au deposition on the substrate, giving smaller diameters of holes corresponding to the original size of the larger particles. The detailed mechanism for Au footprint formation through a binary colloidal layer is currently unknown; however, the hypothesis is that the atoms reach the substrate by diffusion through the voids of the small particles or the crystals of the small particles can allow diffusion of the energetic species. The entire surface area of the substrate under the binary colloidal crystals is coated except for the area in contact with the large particles.

The lateral dimensions of the patterned features are determined by the size of close-packed large colloidal particles in the BCAs, while the height is controlled by the amount of material deposited, that is, deposition time (*t*). With a BCA mask made from 1 $\mu$m $SO_4$−PS/110 nm $NH_2$−PS particles, the hole size has a diameter of

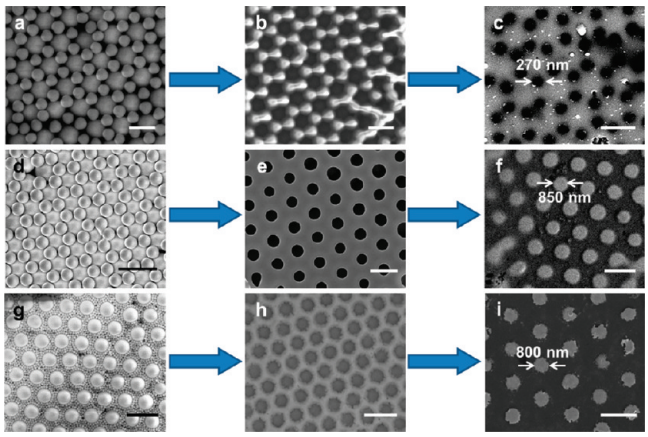


**Figure 4. SEM micrographs showing the generation of different geometries of chemically patterned surfaces using composite BCA masks of high and low size ratios: (a) 1 $\mu$m plain-$SiO_2$ ($\varphi = 5.0 \times 10^{-4}$) and 500 nm $NH_2$—PS ($\varphi = 1.1 \times 10^{-4}$), $\gamma = 0.50$, scale bar = 1 $\mu$m; (b) etching of 1 $\mu$m $SiO_2$ particles after melting the PS particles, scale bar = 1 $\mu$m. (c) The resultant patterned is obtained after Au deposition, and subsequent removal of masks, scale bar = 1 $\mu$m; (d) 2 $\mu$m plain-$SiO_2$ ($\varphi = 4.4 \times 10^{-4}$) and 1 $\mu$m $SO_4$—PS ($\varphi = 2.7 \times 10^{-4}$), $\gamma = 0.50$, scale bar = 3 $\mu$m; (e) etching of 2 $\mu$m $SiO_2$ particles after melting the PS particles, scale bar = 2 $\mu$m. (f) The disklike Au features of sizes ~850 nm are obtained after Au deposition and removal of PS mask, scale bar = 2 $\mu$m; (g) 2 $\mu$m plain-$SiO_2$ ($\varphi = 4.4 \times 10^{-4}$) and 200 nm $NH_2$—PS ($\varphi = 9.5 \times 10^{-5}$), $\gamma = 0.10$, scale bar = 3 $\mu$m. (h) The large particles are etched after the melting of small PS particles, scale bar = 3 $\mu$m. (i) Disklike Au features of sizes ~800 nm after Au deposition and removal of PS masks, scale bar = 2 $\mu$m.**

~590 nm (Figure 2g). The chemical contrasts generated by using BCA masks of combinations 500 nm $NH_2$—PS/60 nm COOH—PS and 200 nm $NH_2$—PS/60 nm COOH—PS show footprints of ~250 nm and ~100 nm, respectively (Figure 2h,i). To determine the Au film thickness, the surface topography of the Au against $SiO_2$ patterns was characterized by tapping-mode atomic force microscopy (TM-AFM). AFM height images of chemical patterns obtained by using a 2 $\mu$m COOH—PS/200 nm $NH_2$—PS mask and its section profile reveal the thickness of Au film to be ~4 nm at $t = 6$ min (see Figure S5a in the Supporting Information). Similarly, the section analysis of the AFM height image of the patterned surface generated from a 1 $\mu$m $SO_4$—PS/110 $NH_2$—PS mask shows a Au film thickness of ~6 nm at $t = 6$ min (see Figure S5b in the Supporting Information).

Furthermore, the diameter of the holes within the patterns can be reduced by simply increasing the deposition time (Figure 3a,b). For example, the reduction in the hole diameters (~1 $\mu$m to ~750 nm) was observed with an increase in the deposition time from $t = 10$ min to $t = 20$ min using a BCA mask composed of 2 $\mu$m COOH—PS/200 nm $NH_2$—PS (Figure 3c,d). This is evidence that lateral diffusion of energetic atoms results in Au deposition on the substrate in the contact area of the large particles.[45] Similarly, the effect of deposition time was also studied on the BCA mask produced from 1 $\mu$m $SO_4$—PS/110 $NH_2$—PS, where the reduction in hole diameters from ~450 nm ($t = 10$ min) to ~200 nm ($t = 20$ min) was observed (Figure 3e,f). Therefore, this technique has significant versatility since it allows the generation of well-defined feature sizes down to 100 nm and below by a simple choice of appropriate lower size ratios of BCA masks ($\gamma \leq 0.30$) and by varying the deposition time.

We also explored the possibility of using a high size ratio ($\gamma = 0.50$) BCA mask. Self-assembly of the two colloidal particles having a large difference in their size results in a distinct morphology of BCA where the small particles occupy the triangular voids generated from the hexagonal arrangement of the large particles (Figure 4a). Here, the diameter of the large particle is 1 $\mu$m, and the diameter of the small particles (500 nm) is comparable to the maximum theoretical diameter of the inscribed circle (~560 nm). Therefore, only one small particle settles within each triangular void centered on an interstice in contact with particles in the adjoining interstices. This type of chemically patterned surface is highly dependent on the morphology of BCA mask ($\gamma = 0.50$), which can easily be tuned in many ways. In the first approach, the large particles in a composite BCA mask fabricated from mixtures of 1 $\mu$m plain-$SiO_2$/500 nm $NH_2$—PS particles are created (Figure 4a). The large particles (1 $\mu$m plain-$SiO_2$) were etched away by 5% hydrofluoric acid (HF) treatment after heat treatment of the PS particles at 100 °C for 10 min (Figure 4b). When this template is coated with Au ($t = 5$ min), a different type of chemically patterned surface is generated after sonication in toluene to remove the PS particles (Figure 4c). The Au/$SiO_2$ patterns consist of six $SiO_2$ holes of diameter ~270 nm arranged in a hexagonal fashion, corresponding to the original position of the 500 nm PS particles on the silicon substrate.

In a second approach, a composite BCA mask produced from 2 $\mu$m plain-$SiO_2$/1 $\mu$m $SO_4$—PS was heat-treated at 120 °C for 45 min to deform the PS particles for making planar contact (Figure 4d). A PS mask comprising holes of diameter ~840 nm forms after the large particles were etched in 5% HF solution

(Figure 4e). The formation of a PS mask was monitored at different heating time periods (see Figure S6 in the Supporting Information). It was found that the PS particles start deformation within 5 min, and their degree of spreading increases with an increase in the heating time influencing the size of the hole. The detailed mechanism of this process is well-described in the previous reports elucidating the role of interfacial energy of particles, and the contact angle between the particle and solid support.[53,54] Finally, disklike Au features of sizes ~850 nm are generated onto a substrate after 5 min of Au deposition through a polymer mask and its removal by sonication in toluene (Figure 4f). Hence, the composite high-size-ratio BCA masks enable the formation of tunable chemical patterns varying from micrometer to nanosized features, which can easily be controlled by processing parameters such as the size of the colloidal particles comprising BCA masks, melting temperature, and time.

Disklike Au patterns can also be created on the substrate from the composite BCA masks ($\gamma \leq 0.30$) with precise control over the dimension of the features. To demonstrate this, BCA masks were made using the 2 $\mu$m plain-$SiO_2$ and 200 nm $NH_2$—PS colloidal particles (Figure 4g). The large particles (2 $\mu$m plain-$SiO_2$) were etched in 5% HF solution after the BCA mask was heated at 120 °C for 30 min (Figure 4h). Here, the PS particles fill the interstitial sites formed by the assembly of the large particles, and the deformation of PS particles occurs above the PS glass transition temperature ($T_g \approx 100$ °C). When the prepared mask is exposed to Au sputtering for 5 min, again disklike Au features of size ~800 nm (center to center distance $\approx 2$ $\mu$m) form on the substrate after the removal of PS masks by 10 min of sonication in toluene (Figure 4i). The size and separation between the Au features can be controlled by the sizes of the large particles in the BCAs. BCAs comprising 1 $\mu$m plain-$SiO_2$/110 nm $NH_2$—PS and 500 nm plain-$SiO_2$/60 nm COOH—PS resulted in Au disks of sizes ~610 nm (center-to-center distance $\approx$ 1 $\mu$m) and ~200 nm (center-to-center distance $\approx$ 500 nm), respectively, over the large areas (see Figure S7 in the Supporting Information).

To demonstrate the applicability of these chemical patterns as a platform for protein patterning, proof of concept experiments were performed with bovine serum albumin (BSA). The Au regions of surfaces were modified selectively with $EG_3$-SAM to prevent proteins sticking and thereby directing adsorption to the unmodified regions of the pattern. XPS was conducted to examine the surface chemistry of Au/$SiO_2$ patterned surfaces. For this, a series of samples were generated from the BCA (2 $\mu$m COOH—PS/200 nm $NH_2$—PS, $\gamma$ = 0.10) masks with constant deposition time, $t$ = 10 min. Table 1 shows the corresponding elemental composition of the patterned surface before and after $EG_3$-SAM modification generated from XPS survey spectra. The observed chemical composition confirms the deposition of Au layer onto the silicon substrate, and the presence of sulfur (S) is evidence of the grafting of the $EG_3$-SAM onto Au regions. In addition, the high resolution C 1s and S 2p spectra also confirmed the successful $EG_3$-SAM grafting (Figure 5a,b). The C 1s spectra consist of two components with the binding energies of ~285.0 eV (C—C/C—H), and ~286.9 eV (C—O—C/C—OH), accounting for carbon atoms in the alkyl chains and in the tri(ethyleneglycol) groups, respectively.[55] The S $2p_{5/2}$ component in the S 2p spectrum has a binding energy of ~162.1 eV

**TABLE 1. Elemental Composition (atomic %) of the Patterned Surface Generated from BCA Masks (2 $\mu$m COOH—PS/200 nm $NH_2$—PS, $t$ = 10 min) before and after $EG_3$-SAM Treatment and Subsequent BSA Adsorption on Chemically Modified Surface**

| sample | C | N | O | S | Au | Si |
|---|---|---|---|---|---|---|
| Au/$SiO_2$ | 26.2 | | 51.5 | | 10.9 | 11.2 |
| Au/$SiO_2$ ($EG_3$-SAM) | 30.7 | | 45.2 | 4.9 | 11.9 | 11.1 |
| Au/$SiO_2$ ($EG_3$-SAM+BSA) | 52.6 | 14.4 | 24.4 | 3.3 | 3.1 | 3.4 |

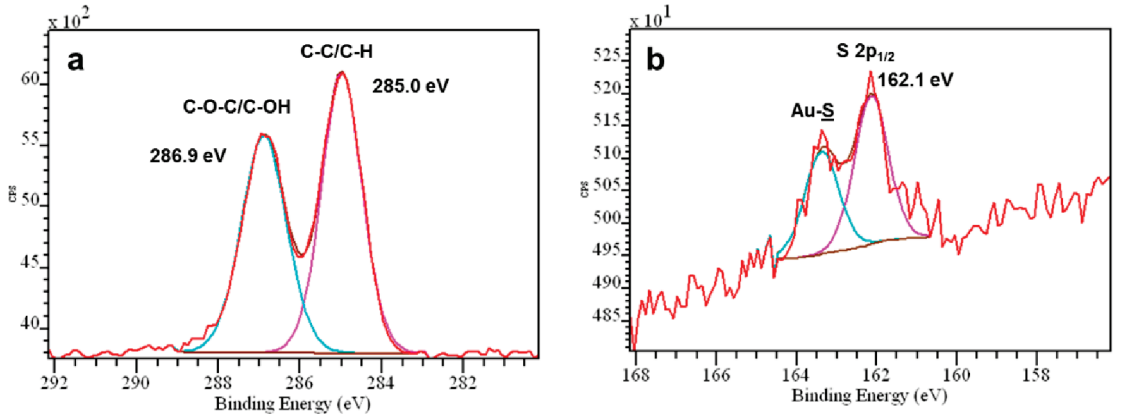


**Figure 5. High resolution XPS spectra of the chemically modified surface generated from 2 $\mu$m COOH—PS/200 nm $NH_2$—PS. (a) C 1s (b) S 2p.**

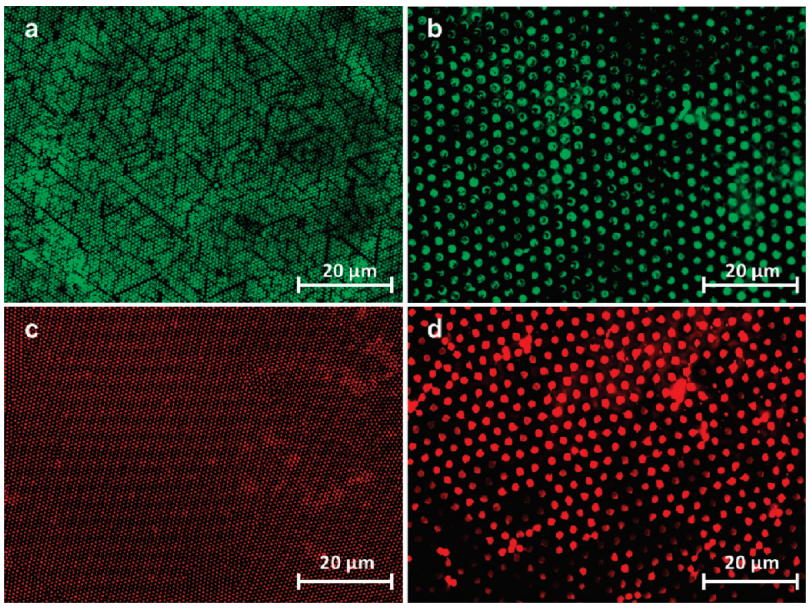


**Figure 6. FM images demonstrate a specific adsorption of R-BSA on unmodified glass regions on different chemical patterns generated from: (a) 2 $\mu$m COOH−PS/200 nm $NH_2$−PS, scale bar = 20 $\mu$m, (b) 5 $\mu$m plain-$SiO_2$/500 nm NH2−PS ($\varphi_{5\ \mu m}$ = 1.4 × $10^{-3}$ and $\varphi_{500\ nm}$ = 1.1 × $10^{-4}$), scale bar = 20 $\mu$m. FM images showing fluorescent signals from disklike Au features on the glass substrate produced from BCA masks: (c) 2 $\mu$m plain-$SiO_2$/200 nm $NH_2$−PS, scale bar = 20 $\mu$m; (d) 5 $\mu$m plain-$SiO_2$/500 nm $NH_2$−PS, scale bar = 20 $\mu$m.**

correspond to the formation of bound Au−S bonds at the SAM/Au interface.[56] When $EG_3$-SAM modified surfaces were exposed to the protein solution of BSA (1 mg/mL in phosphate buffer saline (PBS)) for 2 h under ambient conditions, a sufficient amount of adsorbed protein was detected by XPS (Table 1).

To confirm that the patterns were capable of allowing selective protein adsorption to the unmodified regions, chemically modified patterns were exposed to tetramethylrhodamine-labeled bovine serum albumin (R-BSA) followed by fluorescent microscopy (FM). Figure 6a shows a FM image after R-BSA adsorption to a pattern generated from a 2 $\mu$m COOH−PS/200 nm $NH_2$−PS BCA mask ($\gamma$ = 0.10) with a Au layer deposited at $t$ = 10 min. It is evident that the fluorescent signals are mostly due to R-BSA specifically adsorbing onto the unmodified $SiO_2$ regions within the patterned surface. These protein-coated spots are of sizes ~1 $\mu$m or less and are separated from each other by a distance ~2 $\mu$m corresponding to the original large particles center-to-center distance (SEM micrograph in Figure 2b). The separation between the protein spots and their size can easily be tuned with varying the type of BCA mask. For example, a BCA mask produced from a 5 $\mu$m plain-$SiO_2$ and 500 nm $NH_2$−PS yields ~5 $\mu$m separation of the protein spots with a spot size of ~2.5 $\mu$m on the chemically patterned surface (Figure 6b). We have also generated disklike Au patterns on glass using a composite BCA mask with $\gamma \leq$ 0.30 (as shown in Figure 4i). Here, PEG-silane was used to modify the background substrate and minimize nonspecific BSA adsorption. Figure 6 panels c and d show the specific adsorption of R-BSA onto the disklike Au regions generated from 2 $\mu$m plain-$SiO_2$/200 nm $NH_2$−PS and 5 $\mu$m plain-$SiO_2$/500 nm $NH_2$−PS BCA masks, respectively. Again, the distance and separation between the proteins adsorbed on Au disk regions can be tuned with varying the size of the particles employed during the formation of the BCA masks.

## CONCLUSION

A simple and versatile approach to generate micrometer to nanometer tunable ordered chemical patterns that can be used to create protein patterns, using self-assembled BCA masks against Au sputtering has been successfully demonstrated. The design of the patterned surface is highly dependent on the sizes of colloidal particles employed during the BCA mask formation, their size ratio, and the chemistry of particles, that is, polystyrene or silica. For $\gamma \leq$ 0.30, BCA mask patterns are generated comprising a hexagonal pattern of $SiO_2$ holes with a background of Au. The lateral dimensions of these patterns can be varied with size of the large particles used in the binary colloid and the Au deposition time. BCA masks made from PS and silica particles having $\gamma$ = 0.50 yield multiple chemical patterns (holes or discs), which can be altered by adjusting the temperature when melting the PS particles. We also have shown the use of low size ratio composite BCA masks to generate tunable Au disklike patterns of controllable spacings and sizes. The approach reported here offers several advantages which include the following: precise control of the chemical patterns using colloidal particles of desired size; it is fast and inexpensive, that is, no

sophisticated instrument is required; the method generates nanoscale features employing micrometer sized particles; possibility to produce large area ordered chemical patterns of variable geometries, which is especially important for developing technological applications; and nanopatterning of biomolecules (proteins, DNA and polysaccharides) that is of interest for cell culture dishes, biosensors with improved sensitivity, enhancing immunoreaction efficiency and tissue engineering applications.

## EXPERIMENTAL SECTION

**Materials.** Monodisperse 200 nm $NH_2$−PS particles (2 wt % solid) were purchased from the Polyscience Inc. (USA); 60 nm COOH−PS (4 wt % solid), 110 nm $NH_2$−PS (2 wt % solid), 500 nm $NH_2$−PS (2 wt % solid), 1 $\mu$m $SO_4$−PS (8.3 wt % solid), and 2 $\mu$m COOH−PS (4 wt % solid) were purchased from Invitrogen, USA. One micrometer plain-$SiO_2$ (10% wt solid), 5 $\mu$m plain-$SiO_2$ (10% wt solid), and 500 nm plain-$SiO_2$ (10% wt solid) were received from Microparticles GmbH, Germany, and 2 $\mu$m plain-$SiO_2$ (9.1% wt solid) was purchased from Bang Laboratories, Germany. Ammonium hydroxide, hydrogen peroxide (30%), absolute ethanol (HLPC grade), hydrofluoric acid (40%), and albumin from bovine serum (BSA) (lyophilized powder) were purchased from Sigma Aldrich. $EG_3$-SAM and PEG-silane were used as received from Asemblon Inc. (Germany) and Gelest (USA), respectively. The fluorescent labeled tetramethylrhodamine bovine serum albumin (R-BSA) conjugate was bought as a lyophilized powder from Invitrogen (USA).

**Binary Colloidal Assembly and Chemical Pattern Formation.** Substrates (glass or silicon wafer cut into 1 $cm^2$ pieces) were cleaned by 15 min of sonication each in solutions of ethanol, toluene, and ethanol, followed by drying with $N_2$ gas. All substrates were then UV−ozone treated to remove organic contamination. Highly purified deionized water was used as the solvent during colloidal assembly. The volume of colloidal particle solution ($V_P$), number of the particles in the solution ($N$), and subsequently, their volume fractions ($\varphi$) were calculated assuming the area of substrate encircled by the rubber ring, diameter, and % wt solid content of particles employed (see equations in the Supporting Information). We have also determined the number ratio of large to small particles for different binary colloidal assemblies used in the work (see Table S1 in the Supporting Information). In this method, we used very low amounts of colloidal particles; for instance, to make 200 nm $NH_2$−PS and 2 $\mu$m COOH−PS binary crystals inside a 1 cm diameter rubber ring, 200 nm ($\varphi = 9.5 \times 10^{-5}$) and 1.8 $\mu$L of 2 $\mu$m ($\varphi = 5.3 \times 10^{-4}$) particles were mixed in 100 $\mu$L of highly purified deionized water (0.5 $\mu$S/cm conductivity). They were left for 1 h to allow them to be well dispersed. Rubber rings were cleaned thoroughly by sonication in ethanol for 15 min. After the rubber ring was fixed to the substrate, the colloidal particles suspension was dropped carefully inside the ring. The substrate was then kept in a vacuum desiccator at room temperature until complete evaporation of the solvent, which typically took 2−3 h, depending upon ambient temperature and humidity. An Edwards sputter coater 5150B (Edwards High Vacuum Ltd., UK) was used for the sputtering of gold over the colloidal patterned surfaces (2.5 W, argon pressure of $2 \times 10^{-3}$ bar).

**Grafting and Specific Protein Adsorption.** For grafting of $EG_3$-SAM, the prepared chemically patterned surfaces were cleaned in basic piranha solution (ammonium hydroxide/hydrogen peroxide/purified deionized water, 1:1:5) at 75 °C for 1 h. The cleaned surfaces were rinsed with purified deionized water and dried with $N_2$ gas, and then samples were UV ozone treated for 30 min to remove organic contamination. Immediately, the fresh samples were immersed into an $EG_3$-SAM solution (1 mM solution in absolute ethanol) for 48 h. After thiolation, surfaces were rinsed three times with absolute ethanol and dried with $N_2$. To graft PEG-silane, the Au patterned surfaces were cleaned for 15 min of sonication in ethanol, and afterward these surfaces were kept in UV−ozone treatment for 2 h to achieve a perfect hydrophilic surface and to remove any organic contaminants. The fresh samples were dipped into a prepared 1% PEG-silane solution in toluene for 3 h under ambient conditions. After the surface treatment, the samples were washed twice in toluene for 5 min each, and once in deionized water for 5 min. The freshly grafted samples were exposed to 1 mg/mL R-BSA in PBS (pH = 7.4) for 2 h. After adsorption, samples were rinsed with PBS and purified deionized water to remove loosely bound proteins.

**Characterization Techniques.** Field emission scanning electron microscopy (FEI Nova 600 NanoSEM) was employed for imaging samples using a 5 keV electron source. Prior to imaging, colloidal assemblies were sputtered with gold for 1 min to avoid charging effects. AFM imaging in tapping-mode was performed under ambient conditions at room temperature (23 ± 2 °C) using the Nanoscope III, Digital Instrument, USA. Fluorescent microscopy (Carl Zeiss Axiovert 100, Germany) was used to characterize the protein patterned surface. XPS analyses were performed using a Kratos Axis Ultra DLD spectrometer (Kratos Analytical, UK), equipped with a monochromatized aluminum X-ray source ($Al_{K\alpha}$, $h\upsilon$ = 1486.6 eV) operating at 10 mA and 13 kV (130 W). A hybrid lens (electrostatic and magnetic) mode was employed along with an analysis area of approximately 300 $\mu$m × 700 $\mu$m. Survey spectra were collected over the range of 0−1100 eV binding energy with analyzer pass energy of 160 eV, and high resolution spectra of C 1s and S 2p regions were obtained with an analyzer pass energy of 20 eV. XPS data were processed with Casa XPS software (Casa Software Ltd., UK).

*Acknowledgment.* We thank Jacques Chevallier and Folmer Lyckegaard for their help in experiments. This work was funded through a Danish Research Council Internationalisation Ph.D. Stipend.

*Supporting Information Available:* Equations for DLVO and depletion interaction energies; AFM characterization of gold patterned surface; SEM micrographs of polymer mask formation at different time interval while heating and fabrication of large area disklike Au features; mathematical formula for calculating the colloidal particles concentrations confined in the ring. This material is available free of charge *via* the Internet at http://pubs.acs.org.

## REFERENCES AND NOTES

1. Whitesides, G. M.; Ostuni, E.; Takayama, S; Jiang, X.; Ingber, D. E. Soft Lithography in Biology and Biochemistry. *Annu. Rev. Biomed. Eng.* **2001**, *3*, 335–373.
2. Vo-Dinh, T.; Cullum, B. Biosensors and Biochips: Advances in Biological and Medical Diagnostics. *Fresenius J. Anal. Chem.* **2000**, *366*, 540–551.
3. Chudy, M.; Grabowska, I.; Ciosek, P.; Filipowicz-Szymanska, A.; Stadnik, D.; Wyzkiewicz, I.; Jedrych, E.; Juchniewicz, M.; Skolimowski, M.; Ziolkowska, K.; *et al* Miniaturized Tools and Devices for Bioanalytical Applications: An Overview. *Anal. Bioanal. Chem.* **2009**, *395*, 647–668.
4. Valsesia, A; Colpo, P.; Silvan, M. M.; Meziani, T.; Ceccone, G.; Rossi, F. Fabrication of Nanostructured Polymeric Surfaces for Biosensing Devices. *Nano Lett.* **2004**, *6*, 1047–1050.
5. Volcke, C.; Gandhiraman, R. P.; Basabe-Desmonts, L.; Iacono, M.; Gubala, V.; Cecchet, F.; Cafolla, A. A.; Williams, D. E. Protein Pattern Transfer for Biosensor Applications. *Biosens. Bioelectron.* **2010**, *25*, 1295–1300.
6. Curtis, A.; Riehle, M. Tissue Engineering: The Biophysical Background. *Phys. Med. Biol.* **2001**, *46*, R47–R65.

7. Simon, R.; Mirlacher, M.; Sauter, G. Immunohistochemical Analysis of Tissue Microarrays. *Methods Mol. Biol.* **2010**, *664*, 113–126.
8. Reddy, G.; Dalmasso, E. A. SELDI Protein Chip Array Technology: Protein-Based Predictive Medicine and Drug Discovery Applications. *J. Biomed. Biotechnol.* **2003**, *4*, 237–241.
9. Malmstrom, J.; Christensen, B.; Jakobsen, H. P.; Lovmand, J.; Foldbjerg, R.; Sørensen, E. S.; Sutherland, D. S. Large Area Protein Patterning Reveals Nanoscale Control of Focal Adhesion Development. *Nano Lett.* **2010**, *10*, 686–694.
10. Reyes, C. D.; Petrie, T. A.; Burns, K. L.; Schwartz, Z.; Garcia, A. J. Biomolecular Surface Coating to Enhance Orthopaedic Tissue Healing and Integration. *Biomaterials* **2007**, *28*, 3228–3235.
11. Ito, Y. Surface Micropatterning to Regulate Cell Functions. *Biomaterials* **1999**, *20*, 2333–2342.
12. Kane, R. S.; Takayama, S.; Ostuni, E.; Ingber, D. E.; Whitesides, G. M. Patterning Proteins and Cells Using Soft Lithography. *Biomaterials* **1999**, *20*, 2362–2376.
13. Tai, H. C.; Buettner, H. M. Neurite Outgrowth and Growth Cone Morphology on Micropatterned Surfaces. *Biotechnol. Prog.* **1998**, *14*, 364–370.
14. Torres, A. J.; Wu, M.; Holowka, D.; Baird, B. Nanobiotechnology and Cell Biology: Micro- and Nanofabricated Surfaces to Investigate Receptor-Mediated Signaling. *Annu. Rev. Biophys.* **2008**, *37*, 265–288.
15. Sorribas, H.; Padeste, C.; Tiefenauer, L. Photolithographic Generation of Protein Micropatterns for Neuron Culture Applications. *Biomaterials* **2002**, *23*, 893–900.
16. Qin, D.; Xia, Y.; Whitesides, G. M. Soft Lithography for Micro- and Nanoscale Patterning. *Nat. Protoc.* **2010**, *5*, 491–502.
17. Sun, S.; Montague, M.; Critchley, M.; Chen, M.-S.; Dressick, W. J.; Evans, S. D.; Leggett, G. J. Fabrication of Biological Nanostructures by Scanning Near-Field Photolithography of Chloromethylphenylsiloxane Monolayers. *Nano Lett.* **2006**, *6*, 29–33.
18. Hyun, J.; Ahn, S. J.; Lee, W. K.; Chilkoti, A.; Zauscher, S. Molecular Recognition-Mediated Fabrication of Protein Nanostructures by Dip-pen Lithography. *Nano Lett.* **2002**, *11*, 1203–1207.
19. Hoff, J. D.; Cheng, L.-J.; Meyhofer, E.; Guo, L. J.; Hunt, A. J. Nanoscale Protein Patterning by Imprint Lithography. *Nano Lett.* **2004**, *5*, 853–857.
20. Zhang, G.-J.; Tanii, T.; Zako, T.; Hosaka, T.; Miyake, T.; Kanari, Y.; Funatsu, T.; Ohdomari, I. Nanoscale Patterning of Protein Using Electron Beam Lithography of Organosilane Self-Assembled Monolayers. *Small* **2005**, *1*, 833–837.
21. Blawas, A. S.; Reichert, W. M. Protein Patterning. *Biomaterials* **1998**, *19*, 595–609.
22. Wood, M. A. Colloidal Lithography and Current Fabrication Techniques Producing in-Plane Nanotopography for Biological Applications. *J. R. Soc. Interface* **2007**, *4*, 1–17.
23. Tessier, P. M.; Velev, O. D.; Kalambur, A. T.; Lenhoff, A. M.; Rabolt, J. F.; Kaler, E. W. Structured Metallic Films for Optical and Spectroscopic Applications *via* Colloidal Crystal Templating. *Adv. Mater.* **2001**, *13*, 396–400.
24. Gustavsson, M.; Fredriksson, H.; Kasemo, B.; Jusys, Z.; Kaiser, J.; Jun, C.; Bhem, R. J. Nanostructured Platinum-on-Carbon Model Electrocatalysts Prepared by Colloidal Lithography. *J. Electroanal. Chem.* **2004**, *568*, 371–377.
25. Jiang, P.; Hwang, K. S.; Mittlerman, D. M.; Bertone, J. F.; Colvin, V. L. Template-Directed Preparation of Macroporous Polymers with Oriented and Crystalline Arrays of Voids. *J. Am. Chem. Soc.* **1999**, *121*, 11630–11637.
26. Jiang, P.; Bertone, J. F.; Colvin, V. L. A Lost-Wax Approach to Monodisperse Colloids and Their Crystals. *Science* **2001**, *291*, 453–457.
27. Wright, J. P.; Worsfold, O.; Whitehouse, C.; Himmelhaus, M. Ultraflat Ternary Nanopatterns Fabricated using Colloidal Lithography. *Adv. Mater.* **2006**, *18*, 421–426.
28. Trujillo, N. J.; Baxamusa, S. H.; Gleason, K. K. Grafted Functional Polymer Nanostructures Patterned Bottom-Up by Colloidal Lithography and Initiated Chemical Vapor Deposition (iCVD). *Chem. Mater.* **2009**, *21*, 742–750.
29. Choi, D.-G.; Yu, H. K.; Jang, S. G.; Yang, S.-G. Colloidal Lithographic Nanopatterning *via* Reactive Ion Etching. *J. Am. Chem. Soc.* **2004**, *126*, 7019–7025.
30. Mornet, S.; Bretagnol, F.; Mannelli, I.; Valsesia, A.; Sirghi, L.; Colpo, P.; Rossi, F. Large-Scale Fabrication of Bifunctional Nanostructured Polymer Surfaces for Selective Biomolecular Adhesion. *Small* **2008**, *11*, 1919–1924.
31. Singh, G.; Bremmell, K.; Griesser, H. J.; Kingshott, P. Highly Ordered Nanoscale Chemical and Protein Patterns by Binary Colloidal Crystal Lithography Combined with Plasma Polymerization. *Adv. Funct. Mater.* **2011**, *21*, 540–546.
32. Ray, M. A.; Shewmon, N.; Bhawalkar, S.; Jia, L.; Yang, Y.; Daniels, E. S. Submicrometer Surface Patterning Using Interfacial Colloidal Particle Self-Assembly. *Langmuir* **2009**, *25*, 7265–7270.
33. Ray, M. A.; Jia, L. Micropatterning by Non-Densely Packed Interfacial Colloidal Crystals. *Adv. Mater.* **2007**, *19*, 2020–2022.
34. Isa, L.; Kumar, K.; Müller., M.; Grolig, J.; Textor, M.; Reimhult, E. Particle Lithography from Colloidal Self-Assembly at Liquid−Liquid Interfaces. *ACS Nano* **2010**, *4*, 5665–5670.
35. Bhawalkar, S. P.; Qian, J.; Heiber, M. C.; Jia, L. Development of a Colloidal Lithography Method for Patterning Nonplanar Surfaces. *Langmuir* **2010**, *26*, 16662–16666.
36. Wolf, C.; Li, Q. Tunable Two-Dimensional Array Patterning of Antibody Annuli through Microsphere Templating. *Langmuir* **2010**, *26*, 12068–12074.
37. Taylor, Z. R.; Sanchez, E. S.; Keay, J. C.; Johnson, M. B.; Schmidtke, D. W. Patterning of Quantum Dot Bioconjugates *via* Particle Lithography. *Langmuir* **2010**, *26*, 18938–18944.
38. Chen, J.; Liao, W.-S.; Chen, X.; Yang, T.; Wark, S. E.; Son, D. H.; Batteas, J. D.; Cremer, P. S. Evaporation-Induced Assembly of Quantum Dots into Nanorings. *ACS Nano* **2009**, *3*, 173–180.
39. Xia, Y.; Gates, B.; Yin, Y.; Lu, Y. Monodispersed Colloidal Spheres: Old Materials with New Applications. *Adv. Mater.* **2000**, *12*, 693–713.
40. Velikov, K. P.; Christova, C. G.; Dullens, R. P. A.; van Blaaderen, A. Layer-by-Layer Growth of Binary Colloidal Crystals. *Science* **2002**, *296*, 106–109.
41. Wang, D.; Möhwald, H. Rapid Fabrication of Binary Colloidal Crystals by Stepwise Spin-Coating. *Adv. Mater.* **2004**, *16*, 244–247.
42. Huang, X.; Zhou, J.; Fu, M.; Li, B.; Wang, Y.; Zhao, Q.; Yang, Z.; Xie, Q.; Li, L. Binary Colloidal Crystals with a Wide Range of Size Ratios *via* Template-Assisted Electric-Field-Induced Assembly. *Langmuir* **2007**, *23*, 8695–8698.
43. Denkov, N.; Velev, O.; Kralchevski, P.; Ivanov, I.; Yoshimura, H.; Nagayama, K. Mechanism of Formation of Two-Dimensional Crystals from Latex Particles on Substrates. *Langmuir* **1992**, *8*, 3183–3190.
44. Wang, Y.; Rybczynski, J.; Wang, D. Z.; Ren, Z. F. Large-Scale Triangular Lattice Arrays of Sub-micron Islands by Microsphere Self-Assembly. *Nanotechnology* **2005**, *16*, 819–822.
45. Haynes, C. L.; VanDuyne, R. P. Nanosphere Lithography: A Versatile Nanofabrication Tool for Studies of Size-Dependent Nanoparticle Optics. *J. Phys. Chem. B* **2001**, *105*, 5599–5611.
46. Pan, G.; Kesavamoorthy, R.; Asher, S. A. Nanosecond Switchable Polymerized Crystalline Colloidal Array Bragg Diffracting Materials. *J. Am. Chem. Soc.* **1998**, *120*, 6525–6530.
47. Sperling, R. A.; Rivera, G. P.; Zhang, F.; Zanella, M.; Parak, W. J Biological Applications of Gold Nanoparticles. *Chem. Soc. Rev.* **2008**, *37*, 1896–1908.
48. Wong, L. S.; Khan, F.; Micklefield, J. Selective Covalent Protein Immobilization: Strategies and Applications. *Chem. Rev.* **2009**, *109*, 4025–4053.
49. Bishop, K. J. M.; Wilmer, C. E.; Soh, S.; Grzybowski, B. A. Nanoscale Forces and Their Uses in Self-Assembly. *Small* **2009**, *5*, 1600–1630.
50. Kumnorkaew, P.; Gilchrist, J. F. Effect of Nanoparticle Concentration on the Convective Deposition of Binary Suspensions. *Langmuir* **2009**, *25*, 6070–6075.
51. Yu, J.; Yan, Q.; Shen, D. Co-Self-Assembly of Binary Colloidal Crystals at the Air−Water Interface. *ACS Appl. Mater. Interfaces* **2010**, *2*, 1922–1926.

52. Tohver, V.; Smay, J. E.; Braem, A.; Braun, P. V.; Lewis, J. A. Nanoparticle Halos: A New Colloid Stabilization Mechanism. *Proc. Natl. Acad. Sci. U.S.A.* **2001**, *98*, 8950–8954.
53. Carrillo, J.-M. Y.; Raphael, E.; Dobrynin, A. V. Adhesion of Nanoparticles. *Langmuir* **2010**, *26*, 12973–12979.
54. Lau, A. W. C.; Portigliatti, M.; Raphael, E.; Leger, L. Spreading of Latex Particles on a Substrate. *Europhys. Lett.* **2002**, *60*, 717–723.
55. Kankate, L.; Werner, U.; Turchanin, A.; Golzhauser, A. Protein Resistant Oligo(ethylene glycol) Terminated Self-Assembled Monolayers of Thiols on Gold by Vapor Deposition in Vacuum. *Biointerphases* **2010**, *5*, 30–36.
56. Turchanin, A.; Schnietz, M.; El-Desawy, M.; Solak, H. H.; David, C.; Golzhauser, A. Fabrication of Molecular Nanotemplates in Self-Assembled Monolayers by Extreme-Ultraviolet-Induced Chemical Lithography. *Small* **2007**, *3*, 2114–2119.